



# Research on the blocking effect of baffle-net structure on rock avalanches: consider the influence of particle splashing

Yu-Zhang Bi<sup>1</sup> · Dong-Po Wang<sup>2</sup> · Shuai-Xing Yan<sup>2</sup> · Qin-Ze Li<sup>2</sup> · Si-Ming He<sup>3,4,5</sup>

Received: 10 May 2022 / Accepted: 2 June 2023 / Published online: 28 June 2023  
© Springer-Verlag GmbH Germany, part of Springer Nature 2023

## Abstract

This paper discussed the changes in the movement trajectories and deposition patterns of the rock avalanches in the baffle-net structure under different cases, and obtained the optimal layout parameters of the baffle-net structure in terms of protection effect. The results showed that (1) the particles leaking from the gap between the baffle groups and flowing around the baffle sides were mainly concentrated in Regions I (0~34 cm) and II (34~68 cm) behind the baffles, and the movement range of such particles was relatively small, with low risk; while the splash particles of the rock avalanches were concentrated in Region IV (102~137 cm) behind the baffles, the movement range of such particles was far, with high risk; (2) when the flexible net structure of the first row of baffles was arranged, the blocking rate increased with the increase of the protective net coverage; when the coverage was 100% (case 7), the particle blocking rate behind the baffles reached 52.2%; (3) under the case of 100% coverage, we considered the multi-row baffle-netting, where the case 10 had the highest blocking rate, higher than cases 7, 8, and 9, and the case 10 had the least particle splashing, which was the optimal layout of the baffle-net structure.

**Keywords** Baffle-net structure · Rock avalanches · Particle splash · Blocking rate · Layout optimization

## Introduction

Rock avalanches is a high-risk geological hazard in high mountains and valleys around the world. It has the characteristics of concealment, suddenness, high kinetic energy, high mobility, and extremely high destructive power (Geertsema and Bevington 2020; Fei et al. 2020a; Hungr et al. 2014). In the mountainous regions of southwestern

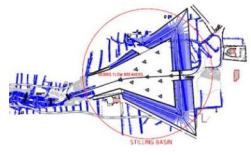
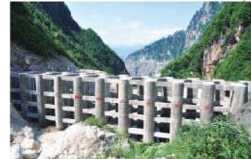

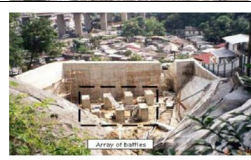

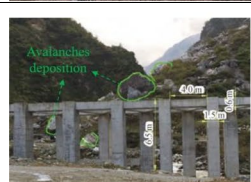
China, the rock avalanches can cause huge property losses and casualties (Zhuang et al. 2019; Luo et al. 2020; Cui et al. 2011; Qi et al. 2011; Zhang and Yin 2013; Zhu et al. 2020). In the practical geo-disaster defending engineering, flexible barriers (Wendeler et al. 2008), check dams (Remaître et al. 2008), and slit dams (Lien 2003) are the usually arranged to protect the residential area.

Due to the complexity and particularity of rock avalanches, ordinary passive structures are not enough to defend this geo-disaster (Bi et al. 2018, 2019; Song et al. 2017; Liu et al. 2020). The baffle group structure is a flow resistance structure with good energy dissipation, drainage, blocking, and interception, which can effectively reduce the kinetic energy of rock avalanches (Bi et al. 2019; Bi et al. 2020; Choi et al. 2014; Choi et al. 2017; Fei et al. 2020b; Wang et al. 2017; Wang et al. 2020; Wang et al. 2021). The use of baffle group system is particularly effective in impeding flow mobility for debris flows (Teufelsbauer et al. 2011; Cosenza et al. 2006), snow avalanches (Hákonardóttir et al. 2001), and water outlets in hydraulic engineering (Thompson and Kilgore 2006). Comparing to other protection methods, the arrays of baffle approach have their unique edge in terms of its low construction cost and strong constructability in complex areas, such as steep natural terrain. Previous studies (Table 1) have shown

✉ Dong-Po Wang  
wangdongpo2014@cdut.edu.cn  
Yu-Zhang Bi  
byz690@yeah.net

<sup>1</sup> College of Civil Engineering, Fuzhou University, Fuzhou 350108, Fujian, China  
<sup>2</sup> State Key Laboratory of Geohazard Prevention and Geoenvironment Protection, Chengdu University of Technology, Chengdu 610059, Sichuan, China  
<sup>3</sup> Key Laboratory of Mountain Hazards and Surface Process, Chinese Academy of Sciences, Chengdu 610041, Sichuan, China  
<sup>4</sup> Institute of Mountain Hazards and Environment, Chinese Academy of Sciences, Chengdu 610041, Sichuan, China  
<sup>5</sup> Chinese Academy of Sciences Center for Excellence in Tibet Plateau Earth Sciences, Beijing 100101, China

**Table 1** Baffle types in practical engineering (redrawn based on Bi et al. (2020))

No.	Location	Type	Description	Photos / Design diagram
1	Wangongji Town, Hanyuan County, Sichuan Province	Array of baffles, Square baffles, Concrete	Two rows, At steep natural terrain	Lack of information
2	Xiaogangjian Village, Tianchi Township, Mianzhu City, Sichuan Province	Array of baffles, Cylindrical baffles, Steel + Concrete	Three rows, At steep natural terrain	Lack of information
3	Montoro Inferiore Area, Southern Italy	Baffles, trapezoidal baffles, Concrete	Four rows, At steep natural terrain	
4	Sanyan Valley, Gansu, China	Baffles-Grille dam system, Cylindrical baffles, Concrete	Two rows, At steep natural terrain	
5	Honghe Creek, Gansu, China	Baffles - Grille dam system, Cylindrical baffles, Concrete	Two rows, at flat deposition area	
6	Sham Tseng, Hong Kong, China	Array of baffles, Square baffles, Concrete	Two rows, at flat deposition area	
7	Dahong Creek, Sichuan, China	Baffles - Grille dam system, Square baffles, Concrete	Two rows, at flat deposition area	
8	Qipan Creek, Sichuan, China	Square baffles, Concrete	Two rows, Interlaced, at flat deposition area	

that baffle group system cannot only installed at flat deposition area, but also installed at steep ground in a natural landslide.

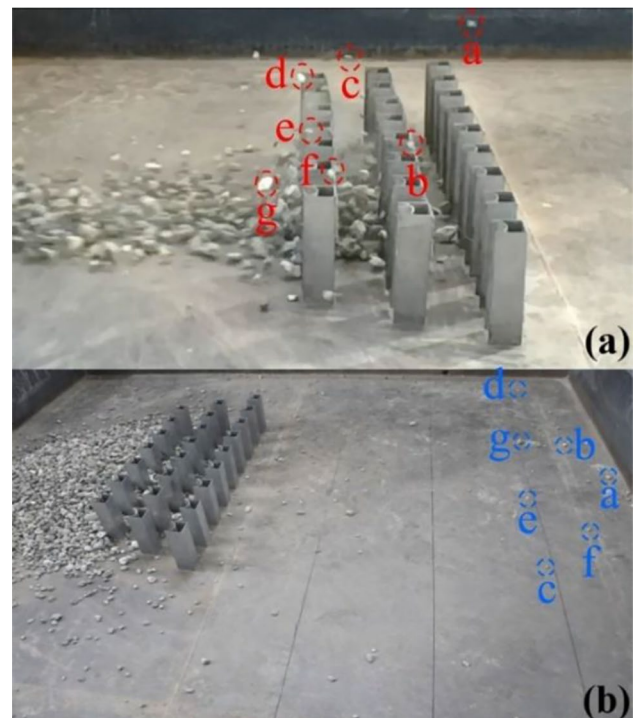
As one of the effective engineering measures for the prevention and control of rock avalanches, the baffle group structure has attracted the attention of many scholars (Bi et al. 2023; Choi et al. 2017; Fei et al. 2020a; Wang et al. 2020). The structure is composed of multiple protection baffles which are arranged in a staggered pattern. When rock avalanches pass by the baffle group, the mutual disturbance between the fluids causes the rock avalanches to slow down sharply, and expands the width of the fluid movement to achieve energy consumption

and disaster reduction. The principle is similar to the function of brake band in road engineering (Bi et al. 2019). Ng et al. (2014, 2015) used staggered baffle group arrays to study the interaction between particle flow and baffle structure through laboratory experiments. They also discussed the influence of the changes in baffle group layout on the particle flow state and downstream deposition length. The test results showed that in order to suppress particle overflow and weaken particle leaping, it was suggested to use the baffles whose height 1.5 times higher than the flow depth. Besides, single-row baffles could barely reduce fluid speed, but increasing the array to three rows could

reduce the downstream impact distance by 65%, and fluid speed by 57%. Choi et al. (2014) studied the influence of baffle group height, row number, and spacing on the flow resistance performance of baffle group through flume test. Huang et al. (2021) used the discrete element method to investigate the influence of baffle groups of different shapes (square and triangle) on the mechanism of rock avalanches, and concluded that square baffles performed better than triangle baffles. Bi et al. (2019) studied the influence of different layouts of baffle groups on the force of rock avalanches impacting baffle groups, and proposed a baffle group-retaining wall structure on this basis. Bi et al. (2019) also optimized the traditional baffle group structure by adding low baffles between the baffle groups to form a speed bump, and used discrete element method for numerical simulation. The results showed that baffle group-speed bump structure could effectively improve the energy consumption effect of the structure. Wang et al. (2020) and Bi et al. (2020) compared and analyzed the three types of baffle group structures, and further carried out the research on the optimization of the arc baffle group layout.

In the previous research by our team, through the physical model test and numerical simulation method of the rock avalanches impacting the baffle group structure, the optimal baffle type, and optimal layout parameters of the baffle group structure were discussed in detail (Wang et al. 2020; Bi et al. 2020). However, it was found in the experiment that even under the optimal layout of the baffle group, many particles still crossed the baffle group system (as shown in Fig. 1). The methods include rolling leakage between baffles, flow around baffles, and particle splashing (Lei et al. 2020). Among them, the splashing particles had less collision with the baffle group and surrounding particles, and the kinetic energy loss was small, the movement trajectory was along the groove direction and the movement distance was long, which meant greater danger. However, the existing baffle group research has not considered particle splashing (Li et al. 2020; Bi et al. 2019; Fei et al., 2020a).

Authors have provided a summary of accidents related to particle splashing, which is presented in Fig. 2. Figure 2(a) illustrates the destruction of a bus caused by a flying rock. On July 11, 2019, a tourist bus was hit by a flying rock on National Highway 213 in Minjiang Township, Songpan County, Sichuan Province, resulting in the death of 8 people and injuries to 16 others. Figure 2(b) depicts splashing rocks flying over a flexible net and falling in a residential area. In October 2018, at the site of Paipa Village, Gangcheng Township, this event caused the death of 2 people and injuries to 3 others. Figure 2(c) shows splashing rocks flying over a flexible barrier and destroying a building structure, which occurred at Tonghua No. 1 Tunnel Entrance from Malkang city to Wenchuan city on July 5, 2022. The disaster in Fig. 2(a) resulted from a rockfall and the original defensive measure was a retaining wall. The disaster in Fig. 2(b) was also caused by rockfall,



**Fig. 1** Rock avalanches impacts the baffle group structure: (a) particle splash; (b) residual particles behind the baffle

and the original defensive measure was a flexible net. The disaster in Fig. 2(c) was due to rock avalanches with a volume of  $0.5 \times 10^4 \text{ m}^3$  and a flow depth of 1.4 m. The original defensive measure was a flexible net.

As the particle splashing is a crucial factor in geo-disaster defending engineering, the studies about the engineering optimization is very necessary. The flexible net should be the effective way to block the flying rocks. However, it is commonly designed using empirical and prescriptive methods since their ability to stop the flying rocks is not well understood (see the cases summarized by authors in Fig. 2). Therefore, this study considers adding a flexible protective net based on the optimal layout of the arc-shaped baffle group to increase the blocking effect of the baffle group. A series of laboratory experiments were conducted by authors, mainly focused on the results of engineering optimization to impede the splashing particles.

## Physical test model

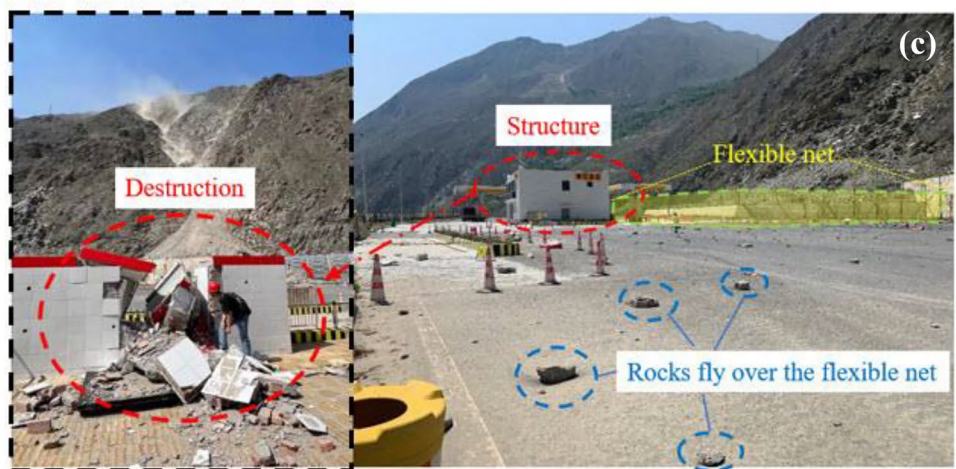
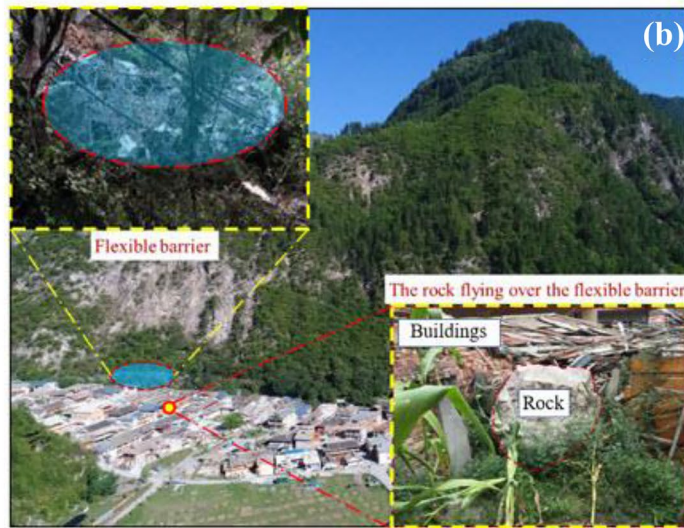
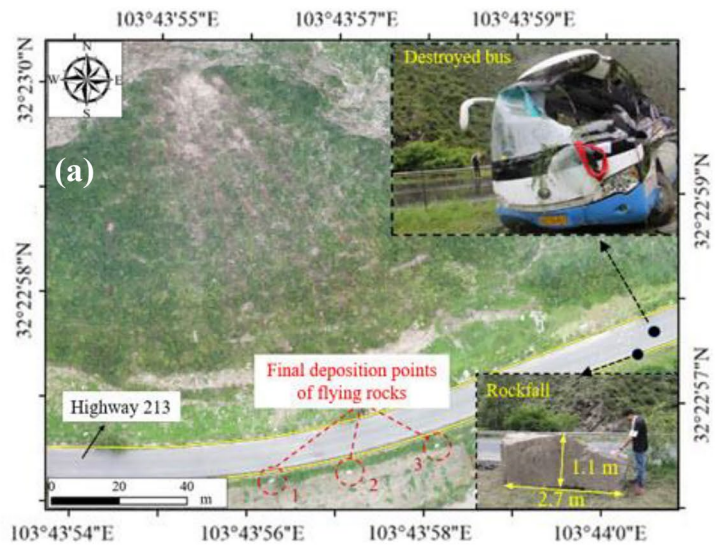
### Test equipment and similarity ratio

#### Test device

The experimental device in this study (shown in Fig. 3) designed based on the predecessor's experimental design



**Fig. 2** Rocks flying over the defending structure and make destruction: **(a)** flying rocks destroy bus; **(b)** flying rocks destroy residential area; **(c)** flying rocks destroy building structure



(Zanuttigh and Lamberti 2006), and the detailed introduction of the device can be found in authors' previous researches (Wang et al. 2020; Bi et al. 2020). Specifically, the provenance region consisted of a rectangular metal bin with a length of 0.4 m, a width of 0.3 m, and a height of 0.9 m, with a capacity of 0.11 m<sup>3</sup>. The bin was 2.5 m away from the ground, which was high enough to meet the gravity potential energy for the movement conditions of the rock avalanches during the test. At the bottom of the bin, an inclined arch-shaped plate was installed to increase the starting angle of the particles to ensure that all particles would be quickly flushed out of the bin, and no residual particles were deposited in the source region. The flow region was composed of a chute with a length of 4.2 m, a width of 0.3 m, a side wall height of 0.5 m, and an inclination angle of 35°. The slope angle of the slope may affect the block effect of the baffle-net structure. This is because the greater the slope angle, the greater the kinetic energy of rock avalanches, which will challenge the block capacity of the baffle-net. Therefore, a fixed slope angle was selected in this study based on practical engineering cases. The effects of different slope angles will be investigated in future studies.

The chute simulated a narrow flow channel of groove-type rock avalanches. The length of the chute was sufficient to accelerate the particles to a flow state that met the test requirements. The buffer deposition area was a square metal platform with 2.5 m long and 2.5 m wide. In the absence of a protective structure, the range of the motion of the particles would not exceed the stacking plane, and there were no particles remaining in the chute, so the size of the device met the hazard range of the rock avalanches in this test. In this test, a high-speed camera was used to record the entire movement of the rock avalanches.

### Similarity ratio

Constructing the model used in this experiment needs to meet three similarities, namely geometric similarity, motion similarity, and dynamic similarity. The detailed description of these similarities can be found in authors' previous researches (Wang et al. 2020; Bi et al. 2020). In this experiment, Froude number was used to study the dynamic similarity between physical model and actual rock avalanches disaster. Froude number is the ratio of inertial force to gravity, which controls the similarity of force in the gravity-driven flow in the groove. In order to carry out the model experiment reasonably, we adopted some similar methods.

Movement and power are similar:

$$(Fr)_m = (Fr)_p = \frac{v_m}{\sqrt{gh_m}} = \frac{v_p}{\sqrt{gh_p}} \tag{1}$$

where  $(Fr)_m$  and  $(Fr)_p$  represent the model Froude number and the prototype Froude number respectively;  $v$  is the fluid faucet speed;  $g$  is the gravity acceleration;  $h$  is the fluid depth.

In the dimensionless equation, the dimensionless number  $(Fr)_p$  is equal to  $(Fr)_m$ . The  $(Fr)_{max}$  of the physical model test in the laboratory was about 6.4, which was equivalent to a prototype groove-type rock avalanches event with a speed close to 35 m/s and a flow depth of about 3 m. The flow conditions are consistent with the debris of the actual case used in this research.

$$(Fr)_{max} = (Fr)_p = 6.4 \tag{2}$$

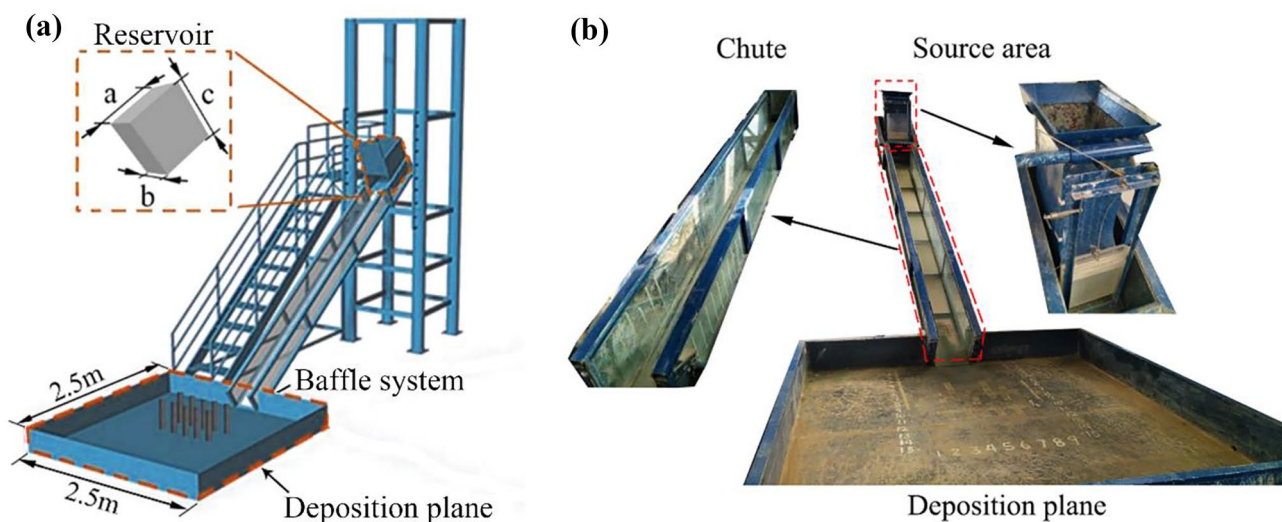
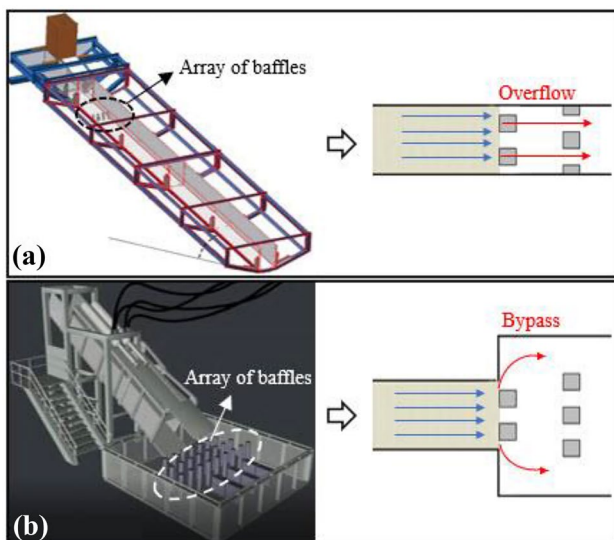


Fig. 3 Physical model test device: (a) schematic diagram of device size; (b) test device



The Froude number adopted in this study is high, some studies imply that the flow is in a supercritical state with quite large runup height (Choi et al. 2016). Choi et al. (2016) proved that the large runup height may induce overflow on top of the barrier to reduce the blocking of the flow. Nonetheless, some studies that related to the array of baffles with high avalanches' Froude number did not have the phenomenon of avalanches overflow (Wang et al. 2020, 2021). This is because that Choi et al. (2016) and Wang et al. (2020) use the different physical model (see in Fig. 4) to make the experiments. Figure 4(a) shows that baffles installed in the chute will make the avalanches overflow the baffles with high Froude number, while Fig. 4(b) shows that some avalanches will not overflow the baffles because the bypass effects will be occurred in the platform. This is because particles have the more disperse deposition under non-constraint conditions, while aggregation effects will be occurred in constraint conditions for avalanches (Bi et al. 2016). In this study, the model that same to the Wang et al. (2020) is used for further studies and the overflow effects will not be discussed in this paper.

Another key dimensionless variable is the ratio between characteristic particle size (PS) and structure opening size (SOS). The spacing between the baffles and the opening size of the flexible net both have an impact on the block effect of rock avalanches. In this paper, however, the term "structure opening size" specifically refers to the spacing between the baffles and does not take into account the opening size of the flexible net. The influence of the opening size of the flexible net on the blocking effect of rock avalanches will be addressed in future studies. The most common method is to take the ratio of SOS length and particle diameter:



**Fig. 4** Different physical model test device: (a) model from Choi et al. (2016); (b) model from Wang et al. (2020)

$$D_{p-s} = \frac{L_{SOS}}{D_p} \quad (3)$$

where the  $D_{p-s}$  is the dimensionless value to determine the SOS;  $L_{SOS}$  is the actual length of SOS (cm);  $D_p$  is the actual diameter of particles. Some researchers use maximum particle diameter (MPD) as the factor to consider the  $D_{p-s}$ , especially in the researches of slit dam (Choi et al. 2016). In the field of dual rigid barriers investigation, the monodisperse particles (Choi et al. 2020) is considered for investigation and  $D_{p-s} = 3$  is suggested to reduce the impact force and overflow volume in their barrier systems. However, in baffles investigation, averaged particle diameter (APD) (Wang et al. 2020) is considered to verify the  $D_{p-s}$ . Wang et al. (2020) have proved that  $D_{p-s} = 3.5$  is the best value for arc-shaped baffles configuration. Hence, the same configuration of Wang et al. (2020) was considered in this study for further investigation.

### Test parameters

The main geometric parameters of the test refer to the optimal layout parameters of the arc-shaped baffle group mentioned in the previous research results by our team (Wang et al. 2020). The baffle height is the most important factor that can affect the results of particle flow protection, especially in order to suppress overflow and reduce runout (Ng et al. 2015). The baffles height is commonly designed based on the maximum particle size and flow depth of avalanches (Choi 2013), which have the deeply relationship with the gravitational potential energy of avalanches (Zhao et al. 2018, Choi 2013). To confirm the baffle size in this study, baffle dimension comparison and rationality analysis were conducted by authors. The following equation can be used to dimensionless analysis:

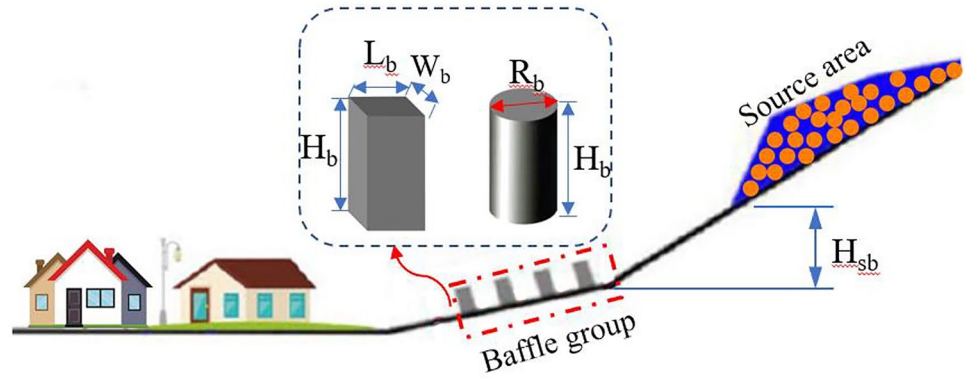
$$H_{dsb} = \frac{H_{sb}}{H_b} \quad (4)$$

where the  $H_{dsb}$  means a dimensionless parameter that used to analyze the baffle size;  $H_{sb}$  means the height from the source area to the baffle group, which affect the gravitational potential energy;  $H_b$  means the baffle height. These size relationships were shown in Fig. 5.

Table 2 shows that the different values of  $H_{dsb}$  in practical engineering and laboratory experiments. Based on previous studies' values in Table 2,  $H_{dsb}$  can be calculated through Eq. (4). The value range of  $H_{dsb}$  is from 3.3 to 36.4. The value of  $H_{dsb}$  in this study is 13.3, which is reasonable for experiments design.

In order to study the impact of particle splashing, this test divided the region behind the baffle group into four regions.

**Fig. 5** Schematic of baffles and source area

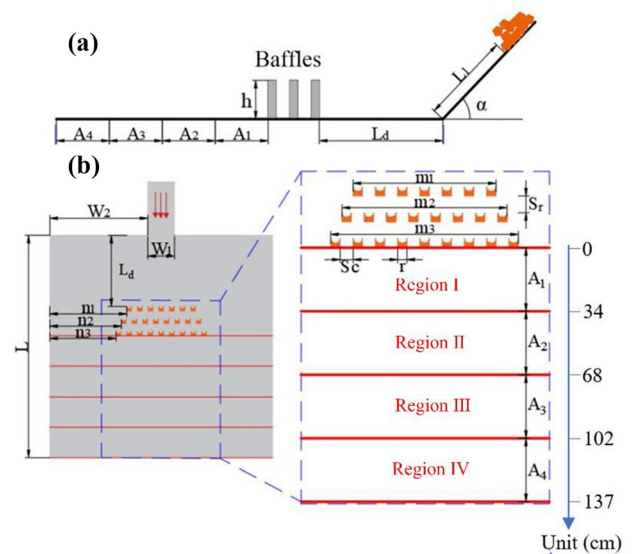


**Table 2** Summarize about the baffle type, baffle size, and the height between the source area and baffles

Scale	Baffle type	Baffle size	Height from the source area to the baffle group ( $H_{sb}$ )	Reference	$H_{dsb}$
Practical engineering	Cylindrical baffles	Height: 8 m; Diameter: 1.5 m	30~50 m	Yang et al. (2014)	3.75~6.25
	Cylindrical baffles	Height: 2.5~6.5 m; Diameter: 1 m	Approximately 80 m	He (2019)	12.3~32
	Square baffles	Height: 4~8 m; Length: 1.5 m; Width: 1.5 m	Approximately 100 m	Zhang et al. (2018)	12.5~25
	Square baffles	Height: 11~35 m; Length: 2.4 m; Width: 1.5 m	Approximately 400 m	Ran et al. (2016)	11.4~36.4
Laboratory experiments	Square baffles	Height: 6~12 cm; Length: 2 cm; Width: 1~2 cm	Approximately 40 cm	Ng et al. (2015)	3.3~6.7
	Cylindrical baffles	Height: 18 cm; Diameter: 2.5 cm	Approximately 240 cm		13.3
	Square baffles	Height: 5 cm; Length: 5 cm; Width: 5 cm	Approximately 80 cm		16

The lengths of Regions I, II, III, and IV were 34 cm, 34 cm, 34 cm, and 35 cm (1.89 h, 1.89 h, 1.89 h, 1.94 h, h is the baffle height) based on the Fig. 6. After each rock avalanches impacted the baffle-net structure, the particle masses in the four regions were recorded. The parameters are shown in Fig. 3 and Table 3. Table 3 shows that  $L_d$  is 0.8 m in the experiment. This parameter would affect the flow behavior of rock avalanches. This is because that increasing the length of  $L_d$  will prolong the friction time between rock avalanches and the ground, resulting in the dissipation of energy in the rock avalanches. In this study, the value of  $L_d$  was mainly based on the experiment conducted by Wang et al. (2020), which was based on the layout of pile groups in actual engineering projects.

The flow behavior of rock avalanches can be affected by various factors, such as the moisture content of the debris. When the debris is dry, it behaves differently compared to when it is saturated with water. Therefore, in this study, the focus was on the dry particle flow behavior of rock avalanches. The particle size used in the experiment was 0.1~30 mm, the average particle size was 2.04 cm, and the total mass was 60 kg. The particle grading curve is shown in



**Fig. 6** Optimal layout of baffle groups and behind-baffle regions (Redrawn based on Wang et al. (2020))

**Table 3** Parameters of the optimal baffle group layout and regions (remade based on Wang et al. (2020))

Names	Symbols	Parameters
Chute angle [°]	$\alpha$	35
Chute length [m]	$L_1$	4.2
Chute width [m]	$W_1$	0.3
Platform length [m]	$L$	2.5
Number of baffle groups	$n$	3
Length between notch and baffle [m]	$L_d$	0.80
Variable of total length of the first row of baffle group [m]	$m_1$	0.77
Variable of total length of the second row of baffle group [m]	$m_2$	0.89
Variable of total length of the third row of baffle group [m]	$m_3$	1.01
Baffle side length/diameter [m]	$r$	0.05
Average particle size [m]	$R$	0.02
Baffle height [m]	$h$	0.18
Baffle spacing [m]	$S_c$	0.07
Row spacing [m]	$S_r$	0.09
Width of Region I [m]	$A_1$	0.34
Width of Region II [m]	$A_2$	0.34
Width of Region III [m]	$A_3$	0.34
Width of Region IV [m]	$A_4$	0.35
Length of $n_1$ [m]	$n_1$	0.86
Length of $n_2$ [m]	$n_2$	0.80
Length of $n_3$ [m]	$n_3$	0.75

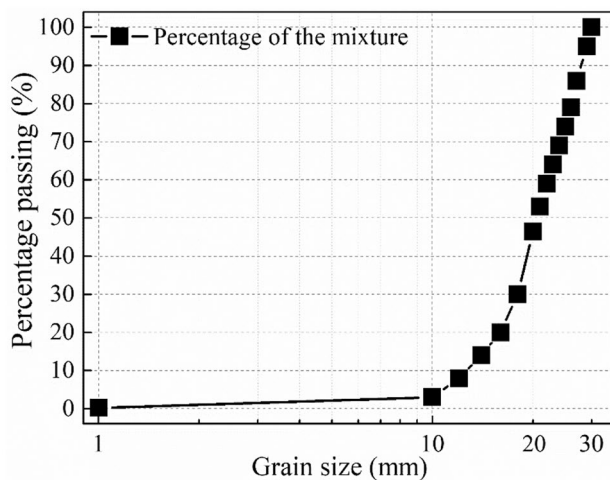
**Fig. 7** Particle grading curve (quoted from Wang et al. (2020))

Fig. 7. According to the particle size, some particles were dyed to better capture the movement trajectory.

The flexible nets used in this study are acquired from Yanhuan New Material Technology Co. LTD. The protection energy against rock avalanches from flexible net itself is 2000 kJ. The stiffness of flexible nets is crucial for protection effects, which has been proved by Song et al. (2017). However, as the scale and impact force of avalanches in this study is too small, the damage and deformation caused to the flexible net by rock avalanches is not considered in this

study. The flexible nets used in this study unveil the effects of blocking particle splashing. The influence of stiffness will not be considered in this study.

### Test scheme

The cases of the experiment are shown in Table 4 and Fig. 8. The main contents of the test are as follows. (1) Carry out the test without nets to restore the optimal layout of the baffle groups before rock avalanches; (2) study only one row of baffles with protective nets (the upper part of the first row of baffles), and when the remaining baffles have no protective nets, compare the blocking efficiency of the structure under different net heights (1/6 h, 1/3 h, 1/2 h, 2/3 h, 5/6 h, 1.0 h, where h is the baffle height); (3) compare the blocking efficiency of the structure under different layout cases when the multiple rows of baffles are simultaneously deployed with protective nets, thereby optimizing the baffle-net structure layout to achieve better blocking effect.

There was a total of 30 test combinations, and each test was repeated 3 times to reduce test errors (the average value of the results in 3 repeated tests was adopted in this study). Cases 2–7 had the same layout, with net on the first row of baffles. Figure 8(a) shows the specific layout of case 4. See Fig. 8(b), (c), (d) for the layout of cases 7, 8, and 10, respectively. Case 9 was similar to case 8, and only the layout of the second row of nets was changed.

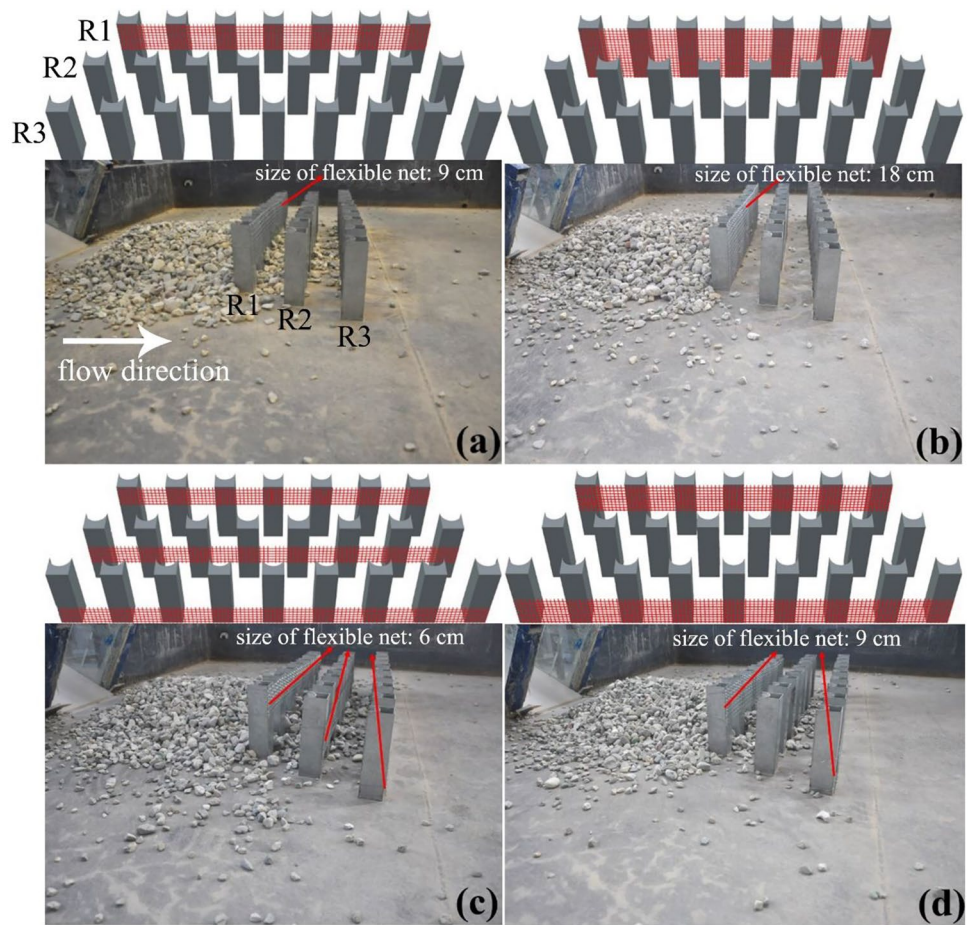


**Table 4** Test parameters

Cases	Protective nets	Coverage (%)	Number of net layers
Case 1	No net	-	-
Case 2	Set a 3 cm net from the top of the baffle in the first row of baffles	16.7	1
Case 3	Set a 6 cm net from the top of the baffle down in the first row of baffles	33.3	1
Case 4	Set a 9 cm net from the top of the baffle down in the first row of baffles	50	1
Case 5	Set a 12 cm net from the top of the baffle down in the first row of baffles	66.7	1
Case 6	Set a 15 cm net from the top of the baffle down in the first row of baffles	83.3	1
Case 7	Set a 18 cm net from the top of the baffle down in the first row of baffles	100	1
Case 8	Set 6 cm nets on the upper part of the first row of baffles, the middle part of the middle baffles and the lower part of the last row of baffles	100	3
Case 9	Set 6 cm nets on the upper part of the first row of baffles, the upper part of the middle baffles and the lower part of the last row of baffles	66.7	3
Case 10	Set 9 cm nets on the upper half part of the first row of baffles, and the lower half part of the last row of baffles	100	2

\*The coverage in the table refers to the area ratio covered by the horizontal protection of the protective net on the baffle group; the number of layers refers to the number of nets arranged on the three-row baffle group

**Fig. 8** Baffle-net structure: (a) case 4; (b) case 7; (c) case 8; (d) case 10



## Test results

Figure 9 shows the distribution of debris after flowing through the baffle group. As shown in the figure, with the third row of baffles as the dividing line, the left side of the baffles is designated as Region A, and the right side is designated as Region B. Among them, the deposition in Region A represents the part of the rock avalanches intercepted by the structure; the deposition in Region B represents the rock avalanches moving outside the protective region through particle turbulence, splashing, passing through baffles, etc. The results of this test will be discussed around the particle distribution in these two regions.

### The blocking effect of the first row of baffles

#### Distribution of the deposition morphology of rock avalanches in Region A

Figure 10 shows schematic about the particles' deposition and distribution. Particles distribution can divide into four parts based on Fig. 10: (1) particles in front of baffles' first row; (2) particles deposited in the baffles group; (3) particles passed through baffles group; (4) splashing particles.

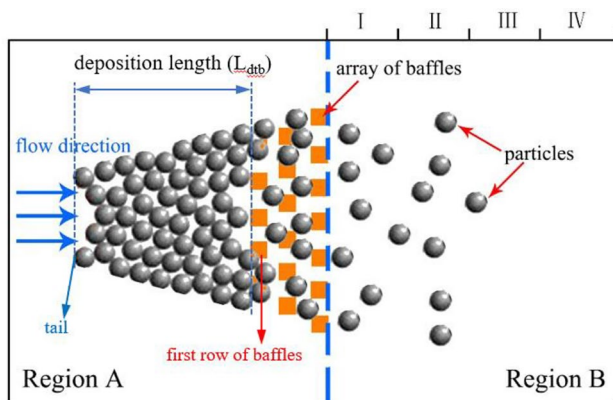
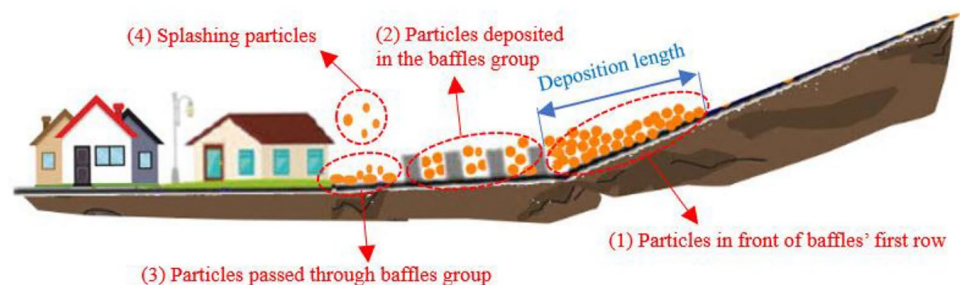


Fig. 9 Schematic diagram of rock avalanches deposition distribution

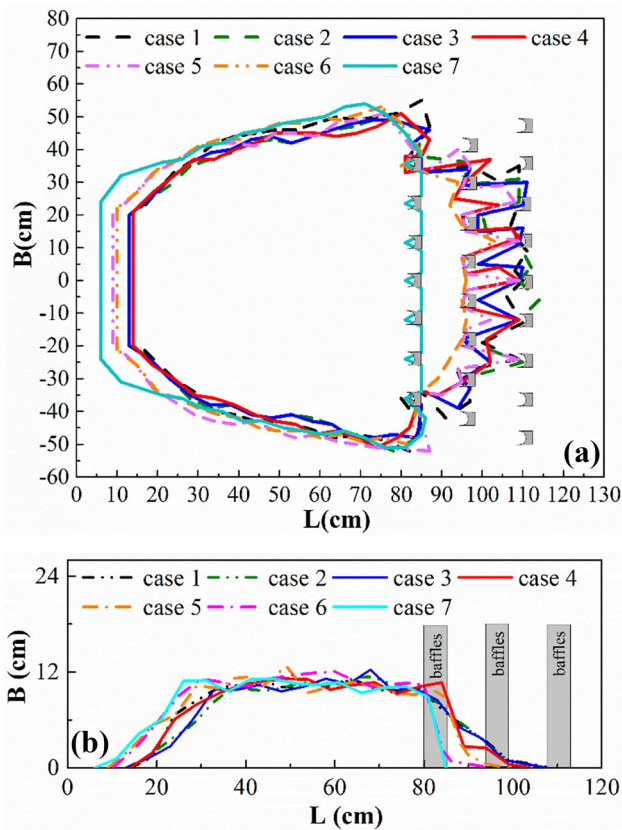
Fig. 10 Schematic about the particles' deposition and distribution



Particles of part (2) and part (3) are needed to pass through baffles group, which may cause more collision and friction between baffles and particles. The part (1) particles did not impact with baffles, which means less energy dissipation compared with particles of part (2) and part (3). Part (4) particles belong to special cases and also have very small percentage of all particles. Thus, if the amount of part (1) particles have a high percentage, it means that the particles amount of part (2) and (3) reduced. The parameters that reflect the amount of part (1) particles can reflect whether the particles have sufficiently collided with the baffles group structure. With the reasons mentioned above, the deposition area and length of part (1) particles are adopted to reflect the circumstance of particles collision with baffles group.

Under the cases 1 to 7, the deposition morphology of rock avalanches impacting the baffle-net structure is shown in Fig. 11. In Fig. 11(a), for the baffle-net structure under cases 1 ~ 7, the deposition areas (top view) in front of the baffles were 5271 cm<sup>2</sup>, 5310 cm<sup>2</sup>, 5328 cm<sup>2</sup>, 5400 cm<sup>2</sup>, 5935 cm<sup>2</sup>, 5936 cm<sup>2</sup>, and 6264 cm<sup>2</sup>. The deposition area in front of the baffles follow these rules: firstly, it decreases with the increase of net size, the deposition area is smallest when the net height is 9 cm; secondly, its area increases with the increase of net size, the deposition area is biggest when the net height is 18 cm. Figure 11(b) shows the comparison of the depth profile of the deposition of particles in front of the baffles under the cases 1 ~ 7. The profile was along the midline of the rock avalanches deposition. The deposition area (side view) under each case was 560 cm<sup>2</sup>, 561.9 cm<sup>2</sup>, 562.4 cm<sup>2</sup>, 581.6 cm<sup>2</sup>, 629.0 cm<sup>2</sup>, 661.6 cm<sup>2</sup>, 672.1 cm<sup>2</sup>, which were similar to the change law of deposition area (side view).

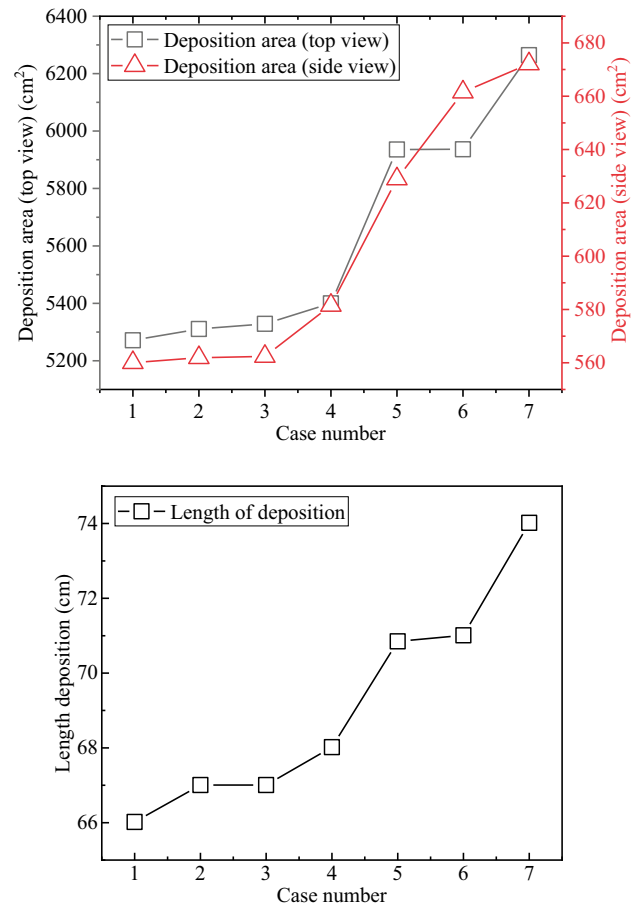
The data on the deposition morphology of rock avalanches was used to draw curves, as shown in Fig. 12. In Fig. 12(a), the difference in the deposition area (top view) in front of the baffles under cases 2, 3, and 4 was small, and the deposition area in front of the baffles was only increased by 0.7%, 1.1%, and 2.4%, respectively compared with that under case 1 (without protective net). Under cases 5, 6, and 7, the deposition area increased by 12.6%, 12.6%, and 18.8% respectively compared with that under case 1. The deposition area (side view) before the baffles under cases 2, 3, and



**Fig. 11** Comparison of the deposition morphology of rock avalanches of the first row of baffles with flexible nets: (a) deposition area (top view); (b) deposition depth (side view)

4 was slightly higher than that under case 1, which was 0.3%, 0.4%, and 3.8% respectively higher than the deposition area before baffles under case 1. Similar to case 1, under cases 5, 6, and 7, the deposition area (side view) in front of the baffles was increased by 12.3%, 18.1%, and 20.0% respectively compared with that under case 1. This is because that the installation of flexible net will make more slashing particles blocked and deposited before the defending structures. With the increase size of flexible net, the more deposition will be formed before the structures.

Furthermore, the deposition length is also investigated in this study and it was defined as the length between the tail deposition and the first row of baffles (see in Fig. 10). In Fig. 12(b), the deposition length of rock avalanches in front of the baffles under cases 2 to 4 was not much different from that under case 1, and only increased slightly by 1.5%, 1.5%, and 3.0%. The deposition length from cases 5 to 7 was increased by 6.1%, 7.7%, and 12.1%, respectively, which show that flexible net installation with multi-row distribution will block more particles before the defending structure. Thus, the less particles should be distributed behind the baffle system.



**Fig. 12** Comparison of the deposition curves of the first row of baffles with nets: (a) deposition area; (b) deposition length

**The distribution law of disaster bodies in Region B**

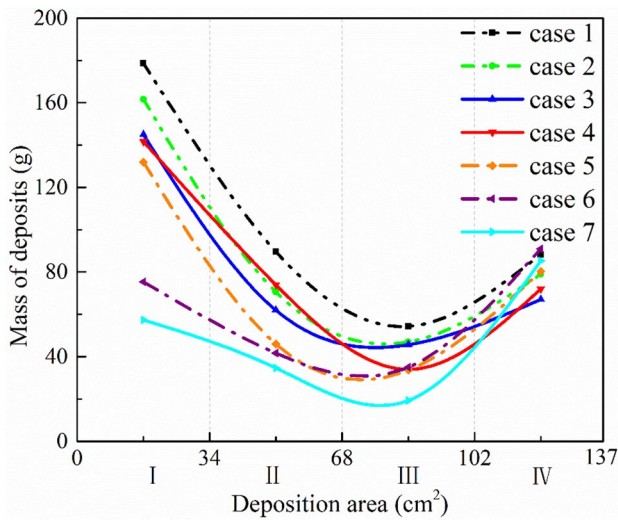
In order to quantitatively analyze the disaster caused by rock avalanches in the region behind the baffles, this test collected the particle masses of the four sub-regions (I, II, III, IV) deposited in Region B (Fig. 9) during each test. The mass of deposited particles in each sub-region is shown in Table 5 and Fig. 13.

Through the images of the high-speed camera (see in Fig. 14), it was found that most of the particles leaking from the flow around the baffle group and rolling between the baffle gaps stayed in Regions I and II (0–3.8 h, h is the baffle height), and a small amount stayed in Region III (3.8–5.7 h). However, the residual particles in Region IV (5.7–7.6 h) were mainly caused by particles splashed by impact. As shown in Fig. 14, when a small number of particles remained in the tail of the rock avalanches, the particles rushed out of the notch and collided with the tail end of the deposition body of rock avalanches particles. The impact changed the direction of movement of the moving particles (flying forward and above in the direction of movement



**Table 5** Particle mass distribution behind the baffles

Cases	Region I (g)	Region II (g)	Region III (g)	Region IV (g)	Total mass (g)
1	178.67	89.67	54.33	88.33	411
2	161.67	70.67	47	79	358.34
3	145	62	45.67	67	319.67
4	141.67	74	34	72	321.67
5	132	46	33.67	80.33	292
6	75.33	41.67	35	91	243
7	57.33	34.67	19.33	85.33	196.66



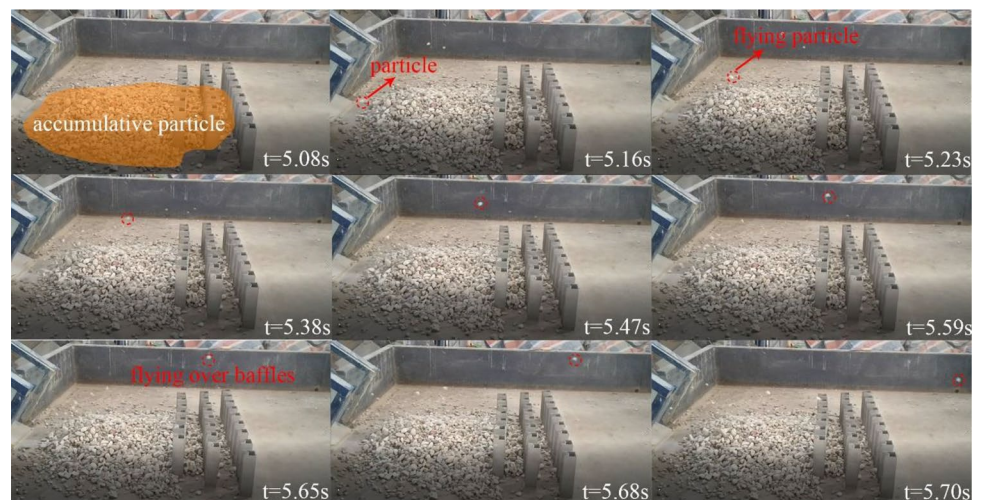
**Fig. 13** Mass distribution in each region behind the baffles

along the rock avalanches). Due to the low resistance in the air, some particles jumped over the baffle-net structure and flew to Region IV (shown in Fig. 15). When the deposition in front of the baffles was getting more serious, the longer the deposition length was, the more splash particles were

produced. In contrast, the particles that flowed around the baffles and the gaps between the baffles were decelerated due to energy dissipation, which was less dangerous. The splash particles generated by the collision maintained a higher speed and were more dangerous.

As shown by the results under cases 1–7, as the coverage of the protective net increased, the particles leaking out between the baffles decreased, and the number of particles in Regions I–III (0–5.7 h) basically decreased. When under cases 6 and 7, the coverage of the protective net was large, the blockage in front of the baffle-net structure was aggravated, and the blocked particles in front of the baffles quickly deposited on both sides, which would cause the particles to bypass the flow path on both sides of the baffle net, and more particles were deposited at the front end of the baffle-net structure, and the particles flowing around the two sides of the baffle-net structure decreased. Therefore, under cases 6 and 7, the particle mass in Region I was reduced by a relatively large value. When a small number of particles remained at the tail of the rock avalanches, the particles rushed out of the notch and collided with the end of the rock avalanches particle deposition body, which changed the direction of movement of the particles. Some particles splashed upwards and crossed the baffle-net structure.

**Fig. 14** Particle leap process



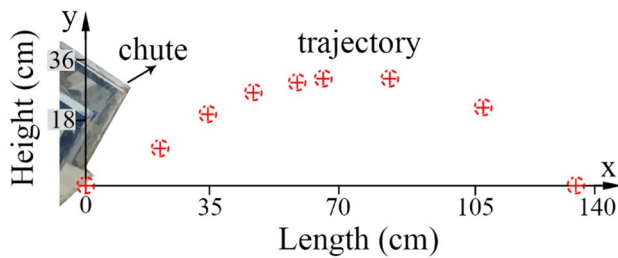


Fig. 15 The trajectory of the particle leap in Fig. 9

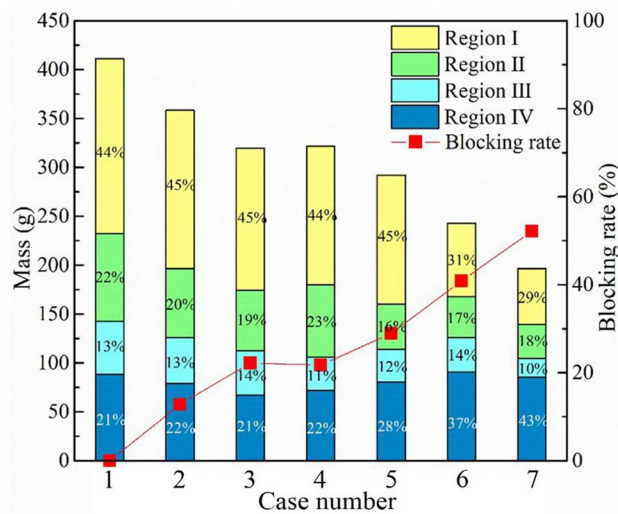


Fig. 16 The particle blocking rate behind the baffles and the percentage of particle mass in each region

This was the main reason for the occurrence of splash particles, and also for the sudden increase in particle mass in Region IV. When the deposition in front of the baffles was getting more serious, the longer the deposition length was, the more splash particles were produced. Therefore, under cases 5–7, as the coverage of the protective net increased, the number of particles deposited in front of the baffles increased, the deposition length ( $L_{dtb}$ ) increased, the number of splash particles generated increased, and the particles in Region IV increased.

In order to further analyze the changes in particle mass in each region, the particle blocking rate behind the baffles and the mass percentage of each region under cases 1 to 7 were calculated, as shown in Fig. 16. The blocking rate  $\eta$  is given by the following:

$$\eta = \frac{w_1 - w_n}{w_1} \times 100\% \tag{5}$$

where  $w_1$  is the total mass of particles behind the baffles under case 1 without protective net;  $w_n$  is the total mass of particles behind the baffles under case  $n$  with protective net.

It can be seen from Fig. 16 that under cases 2–7, the particle blocking rate behind the baffles was increased by 12.8%, 22.2%, 21.7%, 29.0%, 40.9%, and 52.2% respectively compared with that under case 1. As the coverage of the protective net increased, the total mass of particles behind the baffles decreased, and the blocking rate of the baffle-net structure increased. Thus, the differences in particle mass ratio in the 4 regions are changes in absolute percentage instead of percentage changes. The particle mass ratio in different region can be calculated as follows:

$$P_i = \frac{m_i}{m_t} \tag{6}$$

where  $P_i$  means the particle mass ratio in Region I ( $i = 1, 2, 3, 4$ ),  $m_i$  means the particles mass in Region I,  $m_t$  means the total mass in total four regions with different cases.

Under cases 1 to 4, the proportion of particle mass in each region did not change significantly. The mass of particles deposited in Region I took the main proportion, accounting for about 45%; while under cases 5 to 7, as the coverage of the protective net increased, the proportion of particle mass in Region I gradually decreased, and the proportion of particle mass in Region IV increased, gradually becoming the region with the largest mass percentage. Compared with case 1, the particle mass ratio (absolute percentage) in Region I, Region II, and Region III was reduced by 34%, 18%, and 23% respectively under case 7. Meanwhile, compared with case 1, the particle mass ratio in Region IV was increased by 104% under case 7. Therefore, as the coverage of the protective net increased, when the coverage exceeded 50%, the region far behind the baffle-net structure was facing greater threats.

### Summary

Under the same case of setting a net on single-row baffles, the deposition amount in front of the baffles under cases 2–4 had a small difference from that under case 1, and the deposition amount in front of the baffles under cases 5–7 was larger than that under case 1, which was increased by 8.5%, 8.6%, and 14%, respectively. Besides, compared with case 1, the deposition area was increased by 8.1%, 13.7%, and 11.6% respectively, and the deposition length was increased by 7.6%, 6.1%, and 12.1%, respectively. The flow did not sufficiently collide with the latter two rows of baffles. Therefore, under the case with protective net coverage of 0~50% (protective net width was 0~9 cm), for the baffle group structure, the energy consumption and deceleration ability had little effect. When the protective net coverage was

50~100% (protective net width was 9–18 cm), the drainage and energy-consuming deceleration capacity of the baffle group was weakened. In terms of blocking effect, under cases 2–7 (coverage of 16.7–100%), the blocking rate of particles behind the baffles was increased by 12.8%, 22.2%, 21.7%, 29.0%, 40.9%, 52.2%, respectively, compared with that under case 1. Basically, as the coverage increased, the overall blocking effect increased. Although case 7 had a better blocking effect on the rolling leakage of baffles and the particles flowing around the baffles on both sides of the baffles, due to the increase in the amount of deposition in front of the baffles, more and more dangerous splashing particles were generated, and the lower half part of the protective net was directly impacted by the rock avalanches and would withstand greater force.

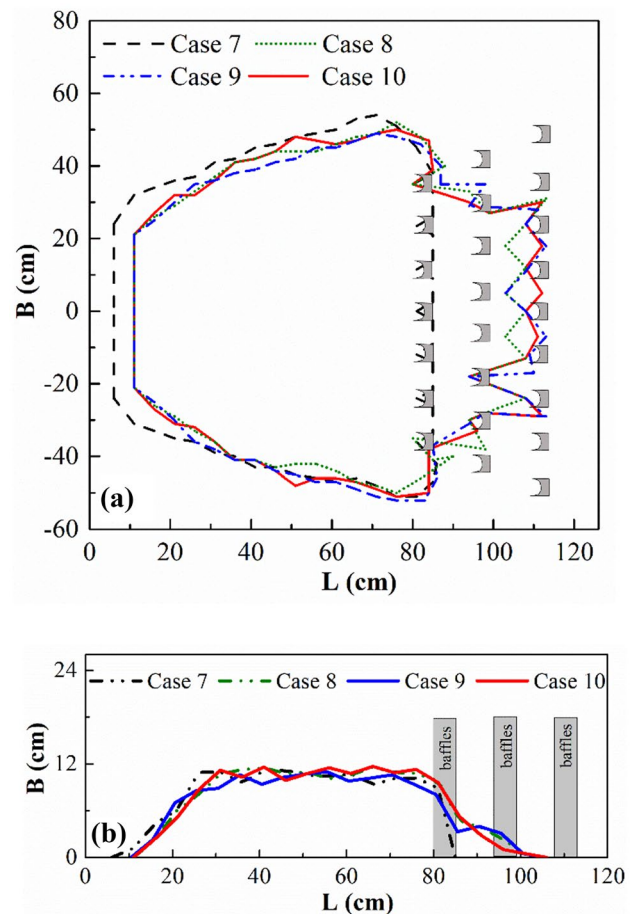
### The blocking effect of multi-row baffles

Because the overall blocking effect of the structure was the best when the protective net coverage was 100%, and at the same time, the protective net coverage was 0–50% (protective net width was 0–9 cm), which had little effect on the drainage of the baffle group and the energy consumption and deceleration capacity, we considered moving the protective net at the bottom of the first row of baffles and arranging them on the second and third rows of baffles to increase the blocking rate, give full play to the drainage effect, and reduce the degree of impact of the protective net at the bottom of the baffle group.

### Distribution of the deposition morphology of rock avalanches in Region A

Under cases 7–10, the deposition morphology of rock avalanches impacting the baffle-net structure is shown in Fig. 17. In Fig. 17(a), under cases 7–10, the deposition area of the particles in front of the baffles was 6268 cm<sup>2</sup>, 5532 cm<sup>2</sup>, 5582 cm<sup>2</sup>, 5652 cm<sup>2</sup>. When the coverage of the baffle-net structure was 100%, the particle deposition area under cases 8 and 10 was lower than that under case 7. Figure 17(b) shows the comparison of the depth profile of the particles in front of the baffles under cases 7–10. The profile was the centerline position of the rock avalanches. The deposition area under each case was 649.3 cm<sup>2</sup>, 644.7 cm<sup>2</sup>, 612.8 cm<sup>2</sup>, and 648.0 cm<sup>2</sup>. The particle deposition area under cases 8 and 10 was not much different from that under case 7.

Particle mass distribution behind the baffles are shown in Table 6. The specific change curve of rock avalanches deposition morphology is shown in Fig. 18. In Fig. 18(a), the particle deposition area in front of the baffles under cases 8, 9, and 10 was reduced by 11.7%, 10.9%, and 9.3% compared



**Fig. 17** Comparison of the deposition morphology of three rows of baffles with nets: (a) deposition area; (b) deposition depth

with that under case 7 (the first row of baffles was equipped with an 18-cm protective net). The deposition area of particles in front of the baffles under case 10 was slightly lower than that under case 7, and for case 9, it was reduced by 5.6%. In Fig. 18(b), the deposition length under cases 8, 9, and 10 was reduced by 6.8%, 6.1%, and 6.8% compared with that under case 7.

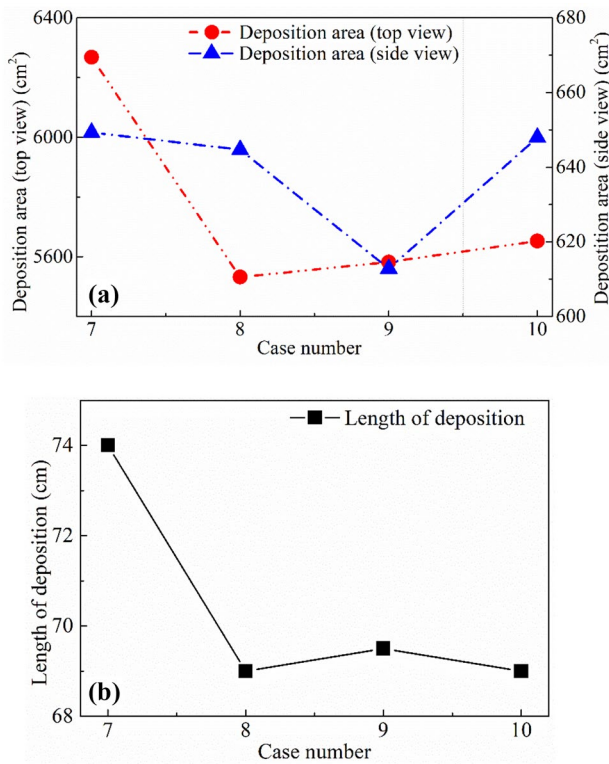
### The distribution law of disaster bodies in Region B

The average deposition mass of particles deposited in the four regions behind the baffle-net structure is shown in Table 4 and Fig. 19. From the perspective of the total mass of particles in each region behind the baffles, case 10 was similar to case 7, while the total mass of particles increased under cases 8 and 9. Compared with case 7, the number of particles in Region IV under cases 8–10 decreased, the regional risk decreased, and the number of particles in Region I increased, and the regional risk increased. The particle masses in Regions II and III under case 10 were the closest to those under case 7, the particle mass under case



**Table 6** Particle mass distribution behind the baffles

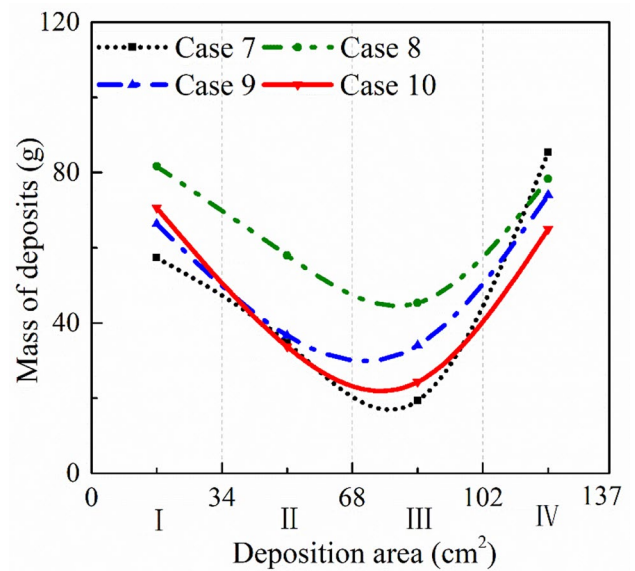
Cases	Region I (g)	Region II (g)	Region III (g)	Region IV (g)	Total mass (g)
7	57.33	34.67	19.33	85.33	196.67
8	81.67	58	45.33	78.33	263.33
9	66.33	36.67	34	74	221
10	70.67	33.67	24.33	65	193.67



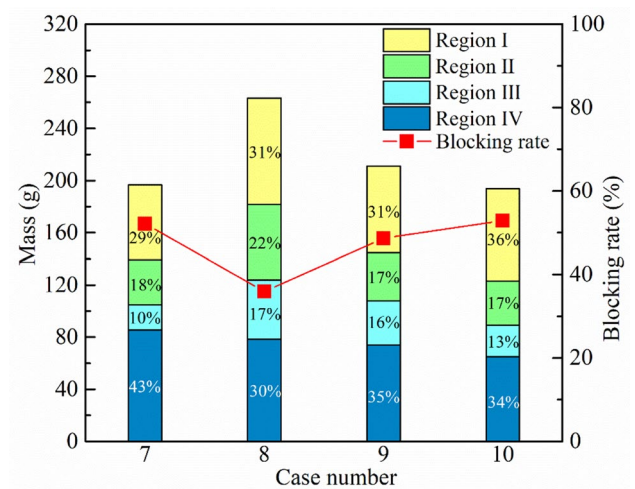
**Fig. 18** Comparison of deposition curves of nets on three rows of baffles: (a) deposition area; (b) deposition length

9 was slightly larger, and that under case 8 was obviously too much.

In order to further analyze the changes in particle mass in each region, this study counted the blocking rate behind baffles and the mass percentage of each region for cases 1 to 7 (shown in Fig. 16). Figure 20 shows that under cases 7–10, the blocking rate behind the baffles was increased by 52.2%, 35.9%, 48.7%, and 52.8%, respectively, compared with the case without a net. The blocking rate of cases 8 and 9 was lower than that of cases 7 and 10. The proportion of particle mass in Region IV under cases 8, 9, and 10 was reduced by 13%, 8%, and 9% respectively compared with that under case 7. Therefore, changing the layout of the protective net could effectively reduce the particle splash effect caused by particle deposition in front of the baffles, and the blocking performance of the baffle-net structure under cases 7 and 10 was better than those under cases 8 and 9.



**Fig. 19** Mass distribution in each region behind the baffles



**Fig. 20** The particle blocking rate and the percentage of particle mass in each region after the multi-baffle net was installed

**Summary**

With the same case with multiple rows of baffles, compared with case 7 (with an 18-cm net in the first row of baffles), the deposition area under cases 8–10 (multiple rows of baffles

were arranged with and 18-cm net) was reduced by 11.7%, 10.9%, and 9.3%, respectively; the deposition area of case 9 was reduced by 5.6%, and the deposition length in front of baffles under cases 8–10 was reduced by 6.8%, 6.1%, and 6.8%. Therefore, the rock avalanche particles under cases 8–10 fully rub and collide with the last two rows of baffles, and the drainage and energy consumption deceleration capabilities of the baffle group could be exerted. Under the conditions of cases 8–10, the blocking rate of particles behind the baffle was increased by 35.9%, 48.7%, and 52.8% respectively compared with than with no net, and the blocking rate of case 10 was slightly higher than that of case 7 at 52.2%. Compared with case 7, the mass and proportion of disaster-causing bodies in Region IV of cases 8–10 had decreased; the mass and proportion of disaster-causing bodies in Region I had increased.

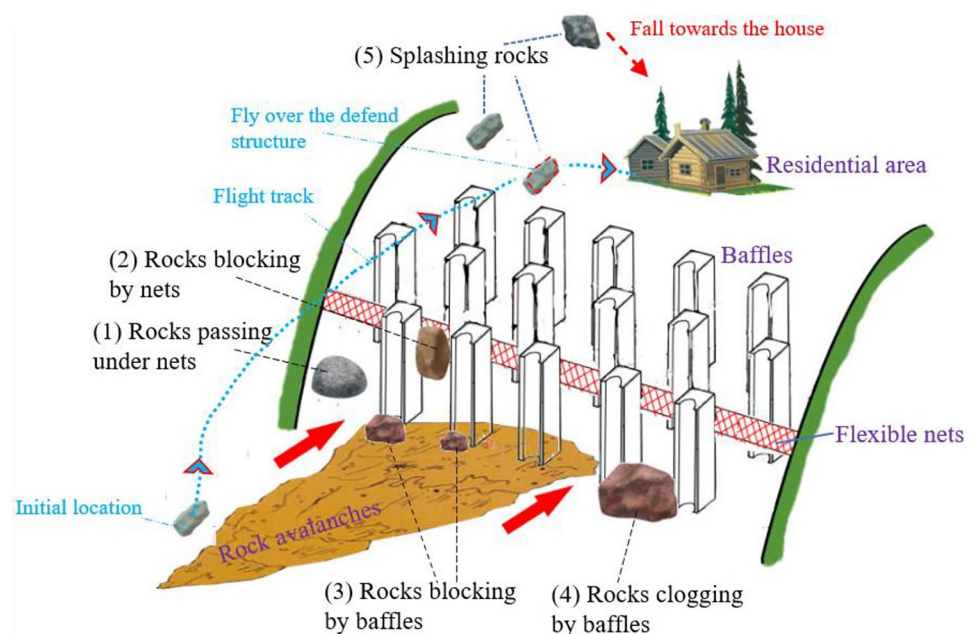
## Discussion

There are five states of rocks during the dynamic response between rock avalanches and baffle-net structure (see Fig. 21) based on the studies: (1) rocks passing under nets, (2) rocks blocked by nets, (3) rocks blocked by baffles, (4) rocks clogged by baffles, (5) rocks splashing through the baffle-net structure. The traditional flexible net may also be able to prevent the rocks from splashing; however, the functions of rocks blocked and clogged by baffles do not exist in traditional flexible net barriers. Moreover, the baffle-net structure can function as an array of baffles (Choi 2013), a flexible net (Kong et al. 2021) and a basal clearance barrier (Choi et al. 2020; Ng et al. 2022). The baffle component of the structure can disrupt the flow of debris, leading

to increased turbulence and energy dissipation, which can help to reduce the velocity and momentum of the rock mass. Meanwhile, the flexible net component of the structure can act as a barrier to intercept and contain the falling rocks, preventing the hazards of rock flying and reducing the damage caused by the rock mass. When the baffle and flexible net components work together, the net beneath can allow the passage of smaller debris, forming a structure similar to a basal clearance barrier, with some of its functions. This innovative baffle-net structure has shown great potential in mitigating the damage caused by rock avalanches and has been widely used in geohazard mitigation accidents, such as rockfall protection systems for roads, railways, and buildings, as well as in slope stabilization and landslide control engineering. Therefore, the baffle-net structure has more advantages to defend the rock avalanches when compared with the traditional flexible net and basal clearance barriers.

The comparison was conducted between case 1 and optimized cases 7 and 10 (see Table 7). From the perspective of the net setting, the lower part of the protective net of the first row of baffles under case 7 was directly impacted by a large number of rock avalanche particles, which was easy to damage, resulting in the inability to exert the blocking effect and causing particle blockage. The protective net of case 10 was arranged at the upper part of the first row of baffles and the lower part of the last row of baffles, and would not be directly impacted by a large number of rock avalanche particles. The deposition phenomenon in front of the baffles under case 7 was obviously more serious than that under case 1. This was because the protective net blocked the rock avalanches out of the first row of baffles, so the drainage and energy-consuming deceleration capabilities of the baffle

**Fig. 21** Five main questions in practical engineering



**Table 7** Comparison of case 1, case 7, and case 10

Description	Case 1	Case 7	Case 10
Protective cloth net	No nets	Set 18-cm nets down from the top of the first row of baffles	Set 9-cm nets on both the upper half of the first row of baffles, and the bottom half of the last row of baffles
Coverage	0	100%	100%
Number of layers	0	1	2
Deposition area in front of the baffles (cm <sup>2</sup> )	5468	6268	5652
Deposition area in front of baffle (cm <sup>2</sup> )	582	649.3	648
Deposition length in front of baffles (cm)	66	74	69
Total mass of particles behind baffles (g)	411	196.67	193.67
Particle blocking rate behind baffles (%)	0	52.2	52.8
Mass of Region I (g)/mass proportion (%)	178.67/44	57.33/29	70.67/36
Mass of Region II (g)/mass proportion (%)	89.67/23	34.67/18	33.67/17
Mass of Region III (g)/mass proportion (%)	54.33/12	19.33/10	24.33/13
Mass of Region IV (g)/mass proportion (%)	88.33/21	85.33/43	65/34

group were not fully utilized. The deposition phenomenon in front of the baffles under case 10 was slightly higher than that under case 1. This was because the rock avalanches were blocked by the lower protective net of the last row of baffles, but the drainage and energy deceleration capacity of the baffle group was basically not affected. The blocking rate behind the baffles of cases 7 and 10 was basically the same, so that the particles behind the baffles were reduced by more than half. Compared with case 7, the proportion of particles in the Region I under case 10 had increased by 7%, and the proportion of particles in Region IV under case 10 had been reduced by 9%. Since the splash particles in Region IV were more dangerous, case 10 was more conducive to blocking the rock avalanches and protecting the rear region. In summary, case 10 was the optimal layout.

## Conclusion

In view of the limitation of the baffle group structure to block particles, a flexible protective net was proposed in this research on the basis of the optimal baffle group layout. By comparing the particle deposition morphology of the rock avalanches, the particle blocking rate behind the baffles, and the particle deposition mass distribution in each region behind the baffles under different protective net layout conditions, the change laws between the layout of protective net, the rock avalanches particle movement and deposition were analyzed. Finally, the optimal layout parameters that not only guaranteed the blocking rate, but also maximized the energy consumption and drainage effect of the structure were obtained. The main conclusions of this research are summarized as follows.

- (1) Most of the particles deposited in Regions I and II after the baffles were formed by the energy consumption deceleration inside the baffle group or flow around the baffle side. Energy was lost during the movement, so the particle speed and risk were both relatively slow. The particles deposited in Region IV behind the baffles were mainly small particles, which were large in number, and the splash speed was relatively fast. The splash direction was directly behind the baffle-net structure, and the energy loss was small and the danger was high.
- (2) The blocking rate of particles behind the baffles increased as the coverage of the protective net increased, and the blocking rate reached 52.2% when the coverage was 100%. However, when the coverage of the protective net exceeded 50%, the degree of particle blockage in front of the baffles increased, which weakened the drainage, energy consumption, and deceleration capacity of the baffle group structure itself, and the blockage in front of the baffles increased the effect of a large number of particles splashing, which posed a threat on the rear remote region of the structure.
- (3) Compared with case 7 (the first row of baffles with and 18-cm net), cases 8–10 (multiple rows of baffles with a total of and 18-cm net) the degree of particle blockage in front of the baffles was reduced. The blocking rate of cases 7 and 10 was basically the same, which was better than cases 8 and 9, but case 10 produced fewer splash particles in Region IV. Therefore, the layout of case 10 (upper half part of the first row of baffles and the bottom part of the last row of baffles were both equipped with a protective net with a coverage of 50%) was the optimal layout.



**Acknowledgements** The authors thank all anonymous reviewers for helpful suggestions.

**Funding** This work was supported by the State Key Laboratory of Geohazard Prevention and Geoenvironment Protection Independent Research Project (SKLGP2021Z001), Sichuan Science and Technology Plan Project (2023YFS0444), National Key Research and Development program of China (Project No.2022YFF0800604), the Major Program of the National Natural Science Foundation of China (Grant No.42090051), and the National Natural Science Foundation of China (Grant No. 42207232).

**Data availability** The data that support the findings of this study are available from the corresponding author, Dongpo Wang, upon reasonable request.

## References

- Bi YZ, He SM, Li XP (2016) Kinetic mechanism of mixed particles under constraint conditions[J]. *Chin J Geotech Eng* 38(3):529–536 (in Chinese)
- Bi YZ, Du YJ, He SM et al (2018) Numerical analysis of effect of baffle configuration on impact force exerted from rock avalanches[J]. *Landslides* 15(5):1029–1043. <https://doi.org/10.1007/s10346-018-0979-z>
- Bi YZ, He SM, Du YJ et al (2019) Effects of the configuration of a baffle–avalanche wall system on rock avalanches in Tibet Zhangmu: discrete element analysis[J]. *Bull Eng Geol Env* 78(4):2267–2282. <https://doi.org/10.1007/s10064-018-1284-8>
- Bi YZ, Sun XP, Zhao HZ et al (2020) Comparison regarding the effects of different baffle systems as impacted by rock avalanches[J]. *Int J Civil Eng* 1–18. <https://doi.org/10.1007/s40999-020-00557-w>
- Bi YZ, Wang XY, Wang DP et al (2023) A Methodological Study on the Design Defending Baffles Based on Mangrove Bionics[J]. *Buildings* 13(2):310. <https://doi.org/10.3390/buildings13020310>
- Choi CE, Ng CWW, Song D et al (2014) Flume investigation of landslide debris–resisting baffles[J]. *Can Geotech J* 51(5):540–553
- Choi CE, Ng CWW, Goodwin GR et al (2016) Flume investigation of the influence of rigid barrier deflector angle on dry granular overflow mechanisms[J]. *Can Geotech J* 53(10):1751–1759
- Choi CE, Cui Y, Liu LHD et al (2017) Impact mechanisms of granular flow against curved barriers[J]. *Géotechnique Lett* 7(4):330–338
- Choi CE, Ng CWW, Liu H et al (2020) Interaction between dry granular flow and rigid barrier with basal clearance: analytical and physical modelling[J]. *Can Geotech J* 57(2):236–245
- Choi CE (2013) Flume and discrete element investigation of granular flow mechanisms and interaction with baffles[D]. The Hong Kong University of Science and Technology p 120–135
- Cosenza E, Cozzolino L, Pianese D et al (2006) Concrete structures for mitigation of debris–flow hazard in the Montoro Inferiore Area, Southern Italy[C]. 2nd International Congress, IFSC, Naples, p 1–12
- Cui P, Chen XQ, Zhu YY et al (2011) The Wenchuan earthquake (May 12, 2008), Sichuan province, China, and resulting geohazards[J]. *Nat Hazards* 56(1):19–36
- Fei J, Jie Y, Sun X et al (2020a) Experimental investigation on granular flow past baffle piles and numerical simulation using a  $\mu$  (I)-rheology-based approach[J]. *Powder Technol* 359:36–46
- Fei JB, Jie YX, Hong CY et al (2020b) Modelling of avalanche–obstacle interaction using the depth-averaged continuum approach[J]. *Granular Matter* 22(2):1–15
- Geertsema M, Bevington A (2021) A cautionary note for rock avalanche field investigation: recent sequential and overlapping landslides in British Columbia. *Canadian Geotechnical Journal* 58(5):737. <https://doi.org/10.1139/cgj-2019-0751>
- Hákonardóttir KM, Jóhannesson T, Tiefenbacher F et al (2001) A laboratory study of the retarding effect of breaking mounds in 3, 6 and 9 m long chutes[M]. *Veðurstofa Íslands*, p 21–41
- He T (2019) Research on characteristics and treatment of Qifenshui village debris flow in Guilin[D]. Guilin University of Technology (in Chinese), 40–51
- Huang Y, Zhang B, Zhu C (2021) Computational assessment of baffle performance against rapid granular flows[J]. *Landslides* 18:485–501
- Hungr O, Leroueil S, Picarelli L (2014) The Varnes classification of landslide types, an update[J]. *Landslides* 11:167–194
- Kong Y, Li X, Zhao J (2021) Quantifying the transition of impact mechanisms of geophysical flows against flexible barrier[J]. *Eng Geol* 289:106188
- Lei M, Yang P, Wang Y et al (2020) Numerical analyses of the influence of baffles on the dynamics of debris flow in a gully[J]. *Arab J Geosci* 13(19):1–15
- Li X, Yan Q, Zhao S et al (2020) Investigation of influence of baffles on landslide debris mobility by 3D material point method[J]. *Landslides* 17:1129–1143
- Lien HP (2003) Design of slit dams for controlling stony debris flows[J]. *Int J Sedim Res* 18(1):74–87
- Liu C, Yu Z, Zhao S (2020) Quantifying the impact of a debris avalanche against a flexible barrier by coupled DEM–FEM analyses[J]. *Landslides* 17(1):33–47
- Luo JY, Xu ZM, Ren Z et al (2020) Quantitative assessment of weathering degree of the Touzhai rock–avalanche deposit in Southwest China[J]. *Geomorphology* 359
- Ng CWW, Choi CE, Kwan JSH et al (2014) Effects of baffle transverse blockage on landslide debris impedance[J]. *Procedia Earth Planet Sci* 9:3–13
- Ng CWW, Choi CE, Song D et al (2015) Physical modeling of baffles influence on landslide debris mobility[J]. *Landslides* 12(1):1–18
- Ng CWW, Liu H, Choi CE et al (2022) Effects of basal clearance on the impact dynamics of dry granular flow against dual rigid barriers[J]. *Can Geotech J* 99(999):1–14
- Qi S, Xu Q, Zhang B et al (2011) Source characteristics of long runout rock avalanches triggered by the 2008 Wenchuan earthquake, China[J]. *J Asian Earth Sci* 40(4):896–906
- Ran CY, He L, Yu XM et al (2016) Cause analysis and comprehensive post-disaster control of debris flow of Hanyuan Wangong landslide occurred on July 27[J]. *Des Hydroelectric Power Station* 32(1):10–19 (in Chinese)
- Remaître A, Van Asch TWJ, Malet JP et al (2008) Influence of check dams on debris–flow run–out intensity[J]. *Nat Hazard* 8(6):1403–1416
- Song D, Choi CE, Ng CWW et al (2018) Geophysical flows impacting a flexible barrier: effects of solid–fluid interaction[J]. *Landslides* 15:99–110
- Teufelsbauer H, Wang Y, Pudasaini SP et al (2011) DEM simulation of impact force exerted by granular flow on rigid structures[J]. *Acta Geotech* 6(3):119–133
- Thompson PL, Kilgore RT (2006) Hydraulic design of energy dissipators for culverts and channels: hydraulic engineering circular number 14[R]. National Highway Institute (US), p 74–86
- Wang F, Chen X, Chen J et al (2017) Experimental study on a debris–flow drainage channel with different types of energy dissipation baffles[J]. *Eng Geol* 220:43–51
- Wang D, Li Q, Bi Y et al (2020) Effects of new baffles system under the impact of rock avalanches[J]. *Eng Geol* 264:105261
- Wang D, Bi Y, Li Q et al (2021) Kinetic response analysis of different types of baffle submitted to rock avalanches based on discrete element method[J]. *Environ Earth Sci* 80(17):1–21

- Wanze Z, Haifeng H, Wei K et al (2018) Failure mode and optimization analysis of pile structure under the impact action of boulders in debris flow[J]. *Sci Technol Eng* 18(4):15–22 (in Chinese)
- Wendeler C, Volkwein A, Roth A et al (2008) Hazard prevention using flexible multi-level debris flow barrier[C]. 11th Interpraevent Congress, Interpraevent, Dornbirn, Austria, p 547–554
- Yang DX, Wang WG, Cheng XQ (2014) Steel pipe piles used for countermeasures in narrow-steep debris flow gullies: a case study of Xiaogangjian debris flow control[J]. *J Mt Sci* 32(1):74–80 (in Chinese)
- Zanuttigh B, Lamberti A (2006) Experimental analysis of the impact of dry avalanches on structures and implication for debris flows[J]. *J Hydraul Res* 44(4):522–534
- Zhang M, Yin Y (2013) Dynamics, mobility-controlling factors and transport mechanisms of rapid long-runout rock avalanches in China[J]. *Eng Geol* 167:37–58
- Zhao T, Crosta GB, Dattola G et al (2018) Dynamic fragmentation of jointed rock blocks during rockslide-avalanches: insights from discrete element analyses[J]. *J Geophys Res: Solid Earth* 123(4):3250–3269
- Zhu L, Liang H, He S et al (2020) Failure mechanism and dynamic processes of rock avalanche occurrence in Chengkun railway, China, on August 14, 2019[J]. *Landslides* 17(4):943–57
- Zhuang Y, Xu Q, Xing A (2019) Numerical investigation of the air blast generated by the Wenjia valley rock avalanche in Mianzhu, Sichuan, China[J]. *Landslides* 16(12):2499–2508

Springer Nature or its licensor (e.g. a society or other partner) holds exclusive rights to this article under a publishing agreement with the author(s) or other rightsholder(s); author self-archiving of the accepted manuscript version of this article is solely governed by the terms of such publishing agreement and applicable law.